# Many-body effects in molecular photoionization in intense laser fields; time-dependent Hartree–Fock simulations

Masato Suzuki[a)]
*Department of Physics, Graduate School of Science, Osaka City University, 3-3-138 Sugimoto, Sumiyoshi-ku, Osaka, 558-8585, Japan, and Department of Chemistry, University of Rochester, Rochester, New York 14627*

Shaul Mukamel
*Department of Chemistry and Department of Physics and Astronomy, University of Rochester, Rochester, New York 14627*

(Received 23 May 2003; accepted 14 October 2003)

The time evolution of the reduced single electron density matrix for eight electrons in a one-dimensional finite box potential driven by an intense laser field is calculated by numerically integrating the time-dependent Hartree–Fock equations. We study the effects of the Coulomb interaction, field intensity, and frequency on the time profile of the ionization process. Our computed saturation ionization intensity ($I_{sat}$) is in good agreement with experimental results for decatetraene [Ivanov *et al.* J. Chem. Phys. **117**, 1575 (2002)]. © *2004 American Institute of Physics.*
[DOI: 10.1063/1.1631252]

## I. INTRODUCTION

The interaction of various types of materials with intense femtosecond laser pulses has drawn considerable recent theoretical and experimental attention.[1] Multiphoton dissociation and ionization of molecules in strong laser fields allow one to probe and control electronic and nuclear dynamics by electric forces.[2] The coherent creation of multiexcitons by high-density photoexcitations in insulators provides a window into many-body effects among photogenerated elementary excitations.[3]

The interaction of materials and laser fields depends on four basic parameters: field intensity $I$, field frequency $\Omega$, material size (atoms, molecules, polymers, or bulk), and relevant time scale (electron dynamics, phonon dynamics, lattice relaxations, and so forth). For weak $I$, the interaction of an electron or a phonon with a photon can be treated perturbatively, and all effects can be understood by the linear response to the field. In contrast, when the field becomes comparable to internal Coulomb fields, at intensities exceeding $10^{14}$ W/cm$^2$, the response may no longer be described perturbatively in the field and nonlinear phenomena dominate the matter/laser field interaction.

In this study, we focus on molecules driven by a nonresonant ultrashort strong laser field. Recently, intense field dissociation and ionization processes in conjugated polyatomic molecules, such as benzene, naphthalene, anthracene, hexatriene, decatetraene, and $C_{60}$, have been reported.[4–12] In the low-frequency (electronically off-resonant) regime, ionization can be understood qualitatively in terms of a quasistatic tunneling model based on the adiabatic response of a single active electron.[13–15] However, in polyatomic molecules, many-body effects strongly influence the electron dynamics, and electrons are emitted through nonadiabatic multielectron excitation processes.[11,12,16] In small molecules, such as $H_2$ or HCl, when the number of participating electrons is limited to one or two, exact numerical simulation of these processes have been carried out.[16–21] Such calculations are too expensive for polyatomic molecules. Ivanov *et al.*[12] studied this strong excitation process in a polyatomic molecule with eight electrons using a theory which includes the electron–electron Coulomb interaction, but neglects exchange.[12]

In a previous paper, we reported the charge and the bonding redistribution in an octatetraene driven by a strong laser field using the Pariser–Parr–Pople model Hamiltonian[22] and a time-dependent Hartree–Fock (TDHF) simulation in the preionization regime. In the present article, we extend that study to the nonperturbative electronic response of many-electron systems to strong external fields, including multiple-electron excitation induced by both Coulomb and exchange interactions. We simulate the ionization dynamics in polyatomic molecules subjected to a strong femtosecond laser field using a model with eight electrons in a one-dimensional finite potential well by solving the TDHF equations for the single-electron density matrix. Although this level of theory fully includes exchange and provides an approximate treatment of correlations, the TDHF has not proven to be very accurate for atoms,[23–27] but it is not clear how accurate it is for conjugated molecules.

## II. MODEL AND TIME-DEPENDENT HARTREE–FOCK SIMULATIONS

Our simulations of field-induced ionization processes in the multielectron systems start with the one-dimensional Hamiltonian.

a)Electronic mail: suzuki@sci.osaka-cu.ac.jp

 

$$H=\int \Psi^{\dagger}(x)\left[-\frac{\hbar^2}{2m}\Delta\right]\Psi(x)dx+\int \Psi^{\dagger}(x)U_0(x)\Psi(x)dx + \frac{1}{2}\int\int \Psi^{\dagger}(x)\Psi^{\dagger}(x')V(x-x') \times\Psi(x')\Psi(x)dxdx'+E(t)\int \Psi^{\dagger}(x)ex\Psi(x)dx, \quad (2.1)$$

where $\Psi(x)$ ($\Psi^{\dagger}(x)$) is the annihilation (creation) field operator and $x$ is the one-dimensional coordinate of the real space. We assumed the following form for the one-dimensional potential energy $U_0(x)$:

$$U_0(x)=U_0\left[\tanh\left\{\theta\left(|x|-\frac{L}{2}\right)\right\}-1\right]\Big/\ 2, \quad (2.2)$$

where $L$ and $U_0$ represent the length and the depth of the box potential, respectively, and $\theta$ is the reciprocal width of the potential edge. This potential is very similar to that used by Ivanov *et al.*[12] The Ohno model was used for the repulsion between electrons at $x$ and $x'$ $V(x-x')$,

$$V(x-x')=\frac{V}{\sqrt{1+((x-x')/a)^2}}, \quad (2.3)$$

where $a$ is a characteristic length and $V$ is the repulsive energy at the same position.

$E(t)$ represents the Gaussian envelope of the external electric field polarized along $x$,

$$E(t)=E\frac{1}{\sqrt{2\pi}\delta}\exp\left[-\frac{(t-t_p)^2}{2\delta^2}\right][\exp(-i\Omega t)+\exp(i\Omega t)], \quad (2.4)$$

where $E$, $\Omega$, $t_p$, and $\delta$ denote the amplitude, carrier frequency, central time, and duration, respectively. $E$ and $\Omega$ are the key parameters which determine the electronic response as discussed above.

In order to solve Eq. (2.1), $\Psi(x)$ is expanded by a complete set of the plane waves ($\equiv\{\varphi_k^{\sigma}(x)\}$),

$$\Psi(x)\equiv\sum_{k,\sigma}\varphi_k^{\sigma}(x)a_{k,\sigma}, \quad (2.5)$$

where $a_{k,\sigma}$ is the annihilation operator of an electron with spin $\sigma$ ($\equiv\alpha,\beta$) at the plane wave with a momentum $k$. $\varphi_k^{\sigma}(x)$ satisfies the following equation:

$$\left[-\frac{\hbar^2}{2m}\Delta\right]\varphi_k^{\sigma}(x)=E_k\varphi_k^{\sigma}(x), \quad (2.6)$$

where

$$\varphi_k^{\sigma}(x)=\frac{1}{\nu^{1/2}}\exp(ikx)|\sigma\rangle \quad (2.7)$$

and

$$E_k=\frac{\hbar^2}{2m}k^2. \quad (2.8)$$

Substituting Eq. (2.5) into Eq. (2.1), we transform the Hamiltonian from the real space representation to $k$ space,

$$H=\sum_{k,\sigma}E_k a_{k,\sigma}^{\dagger}a_{k,\sigma}+\sum_{q,k,\sigma}U(q)a_{k+q,\sigma}^{\dagger}a_{k,\sigma} + \frac{1}{2}\sum_{q,k,k',\sigma,\sigma'}V(q)a_{k+q,\sigma}^{\dagger}a_{k'-q,\sigma'}^{\dagger}a_{k',\sigma'}a_{k,\sigma} + E(t)\sum_{q,k,\sigma}\mu(q)a_{k+q,\sigma}^{\dagger}a_{k,\sigma}, \quad (2.9)$$

where $U(q)$ and $V(q)$ are the Fourier transforms of $U_0(x)$ and $V(x-x')$, respectively,

$$U(q)=\frac{1}{\nu}\int \exp(-iqx)U_0(x)dx, \quad (2.10)$$

$$V(q)=\frac{1}{\nu^2}\int\int \exp(-iq(x-x'))V(x-x')dxdx', \quad (2.11)$$

$\mu(q)$ denote the dipole moment in $k$ space,

$$\mu(q)=\frac{e}{\nu}\int x\exp(-iqx)dx. \quad (2.12)$$

Our simulations focus on the one-electron density operator in $k$ space

$$\hat{\rho}_{k'k}^{\sigma}\equiv a_{k\sigma}^{\dagger}a_{k'\sigma}. \quad (2.13)$$

$\hat{\rho}_{k'k}^{\sigma}$ can be transformed to real space $[\hat{\rho}(x,x')]$ by the Fourier transformation,

$$\hat{\rho}(x,x')\equiv\Psi^{\dagger}(x)\Psi(x') = \sum_{k,k',\sigma}\frac{1}{\nu}\exp(-i(kx-k'x'))\hat{\rho}_{k'k}^{\sigma}. \quad (2.14)$$

The matrix element of the one-electron density operator is defined as $\rho_{kk'}^{\sigma}(t)\equiv\langle\Phi(t)|\hat{\rho}_{kk'}^{\sigma}|\Phi(t)\rangle$, where $|\Phi(t)\rangle$ is the total many-electron wave function.

We have simulated the time evolution starting with the Heisenberg equation of motion for $\rho_{kk'}^{\sigma}(t)$,

$$i\hbar\dot{\rho}_{kk'}^{\sigma}(t)=\langle\Phi(t)|[\rho_{kk'}^{\sigma},H]|\Phi(t)\rangle = \sum_q U(q)[\rho_{k-q,k'}^{\sigma}(t)-\rho_{k,k'+q}^{\sigma}(t)]+\sum_{q,i,\sigma'}V(q)[\langle\hat{\rho}_{k+q,k'}^{\sigma}\hat{\rho}_{i,i+q}^{\sigma'}\rangle-\langle\hat{\rho}_{k,k'+q}^{\sigma}\hat{\rho}_{i,i-q}^{\sigma'}\rangle] + \sum_q V(q)[\rho_{k+q,k'+q}^{\sigma}(t)-\rho_{k,k'}^{\sigma}(t)]+E(t)\sum_q\mu(q)[\rho_{k-q,k'}^{\sigma}(t)-\rho_{k,k'+q}^{\sigma}(t)], \quad (2.15)$$

where $\langle\cdots\rangle \equiv \langle\Phi(t)|\cdots|\Phi(t)\rangle$ is the expectation value with respect to the total wave function. The equations of motion were closed using the TDHF approximation, which assumes that $|\Phi(t)\rangle$ can be expressed by a single Slater determinant at all times. This results in the following factorization of two-electron densities:

$$\langle \hat{\rho}^{\sigma}_{kk'} \hat{\rho}^{\sigma'}_{ij} \rangle = \rho^{\sigma}_{kk'}(t)\rho^{\sigma'}_{ij}(t) - \delta_{\sigma\sigma'}\rho^{\sigma}_{ik'}(t)\rho^{\sigma}_{kj}(t) + \delta_{\sigma\sigma'}\delta_{kj}\rho^{\sigma}_{ik'}(t). \tag{2.16}$$

The TDHF describes quantum fluctuations around the Hartree–Fock ground state; electron correlation effects are taken into account beyond the random phase approximation. In optical properties of molecules and semiconductors, TDHF contains exciton effects which are missing in stationary Hartree–Fock calculations. TDHF contains information about correlations between electrons and holes (i.e., exciton binding energy). Substituting Eq. (2.16) into Eq. (2.15), we obtain the following closed self-consistent nonlinear equations of motion for the one-electron density matrix:

$$i\hbar\dot{\rho}^{\sigma}_{kk'}(t) = \sum_{q} U(q)[\rho^{\sigma}_{k-q,k'}(t) - \rho^{\sigma}_{k,k'+q}(t)] + \sum_{q,i,\sigma'} V(q)[\rho^{\sigma}_{k+q,k'}(t)\rho^{\sigma'}_{i,i+q}(t) - \rho^{\sigma}_{k,k'+q}(t)\rho^{\sigma'}_{i,i-q}(t)] - \sum_{q,i} V(q)[\rho^{\sigma}_{i,k'}(t)\rho^{\sigma}_{k+q,i+q}(t) - \rho^{\sigma}_{i,k'+q}(t)\rho^{\sigma}_{k,i-q}(t)] + E(t)\sum_{q} \mu(q)[\rho^{\sigma}_{k-q,k'}(t) - \rho^{\sigma}_{k,k'+q}(t)]. \tag{2.17}$$

This approach has been widely used for computing the optical response of conjugated molecules by solving the equation perturbatively in the field.[28] In this study, we avoid this expansion and instead directly solve Eq. (2.17) numerically by applying the fourth-order Runge–Kutta technique.[29] We introduce the discrete time series $\{t_0, t_1, t_2, \ldots, t_s, \ldots, t_f\}$, and $\rho^{\sigma}_{kk'}(t_{s+1})$ is generated from the previous $\rho^{\sigma}(t_s)$ as follows:

$$\rho^{\sigma}_{kk'}(t_{s+1}) = \rho^{\sigma}_{kk'}(t_s) + \tfrac{1}{6}\Delta t(\kappa^{\sigma(1)}_{kk'} + 2\kappa^{\sigma(2)}_{kk'} + 2\kappa^{\sigma(3)}_{kk'} + \kappa^{\sigma(4)}_{kk'}), \tag{2.18}$$

where

$$\begin{aligned}
\kappa^{\sigma(1)}_{kk'} &= -\frac{i}{\hbar}F^{\sigma}_{kk'}(\rho(t_s), t_s),\\
\kappa^{\sigma(2)}_{kk'} &= -\frac{i}{\hbar}F^{\sigma}_{kk'}\left(\rho(t_s) + \frac{1}{2}\Delta t\kappa^{(1)}, t_s + \frac{1}{2}\Delta t\right),\\
\kappa^{\sigma(3)}_{kk'} &= -\frac{i}{\hbar}F^{\sigma}_{kk'}\left(\rho(t_s) + \frac{1}{2}\Delta t\kappa^{(2)}, t_s + \frac{1}{2}\Delta t\right),\\
\kappa^{\sigma(4)}_{kk'} &= -\frac{i}{\hbar}F^{\sigma}_{kk'}(\rho(t_s) + \Delta t\kappa^{(3)}, t_s + \Delta t),
\end{aligned} \tag{2.19}$$

and

$$F^{\sigma}_{kk'}(\rho(t), t) \equiv i\hbar\dot{\rho}^{\sigma}_{kk'}(t), \tag{2.20}$$

$$\Delta t \equiv t_{s+1} - t_s. \tag{2.21}$$

The time evolution of the density matrix is computed by direct iteration of Eq. (2.19). The initial values of $\rho^{\sigma}_{kk'}(t)$ $(=\rho^{\sigma}_{kk'}(t_0))$ are determined by the charge distribution of the ground state without an external field which is given by the Hartree–Fock solution of $H$. We verified that this method gives stable solutions even for a very intense field $(\geqslant 10^{15}\ \mathrm{W/cm^2})$ and for field frequencies $\Omega \leqslant 20\,000\ \mathrm{cm^{-1}}$.

## III. RESULTS AND DISCUSSION

The following parameters were used to mimic field-induced ionization processes in polyenes with eight $\pi$-electrons such as octatetraene or decatetraene: $U_0 = 16.0$ eV, $\theta = 5.0\ \mathrm{A}^{-1}$, $L = 13.2$ A, $a = 1.0$ A, and $V = 2.0$ eV. These parameters roughly reproduce the ionization potential energy and electronic level spacings of the linear polyenes that contain eight $\pi$-electrons.[12] The smoothly varying one-dimensional box potential for these values of $U_0$, $\theta$, and $L$ is depicted in Fig. 1 by the dot–dashed line. We set the field parameters to be $t_p = 50$ fs and $\delta = 10$ fs and computed the time evolution of the system until $t = 100$ fs.

In our calculations, we set the length of the outer region to be $4L$, and used periodic boundary conditions. We verified that this size is sufficiently large to describe the time evolution of the ionized electrons from the potential region in 100 fs. We also set $\Delta t$ to be 0.001 fs. We used 101 size grid for $k$, $k = 2\pi/5Ln$, where $n = 0, \pm 1, \pm 2, \ldots, \pm 50$. About 20 h of central processing unit time is expended in calculating the time evolution of the density matrix of this system until 100 fs using a VT-Alpha 600 Work Station.

In the following calculations, we analyze the effects of interelectron interaction $V$, the dependence on the field intensity $I$ $(\equiv \epsilon_0 cE^2/2$, where $\epsilon_0$ is the vacuum permittivity and $c$ is the speed of light in a vacuum), and field frequency $\Omega$ on the ionization dynamics. We further compare the computed saturation intensity of the ionization with experiment.

### A. Effects of electron–electron repulsion

In Fig. 1, we depict the diagonal elements of the density matrix $\rho(x, x, t=0)$, i.e., the charge distribution of the HF ground state, for $V = 0$ (solid line), 2.0 (dotted line), and 4.0 eV (dashed line). When $V = 0$, the eight electron distribution has four peaks. Once the Coulomb interaction $V$ is switched on, these peaks break and the electron distribution spreads out in order to minimize the electron–electron repulsion.

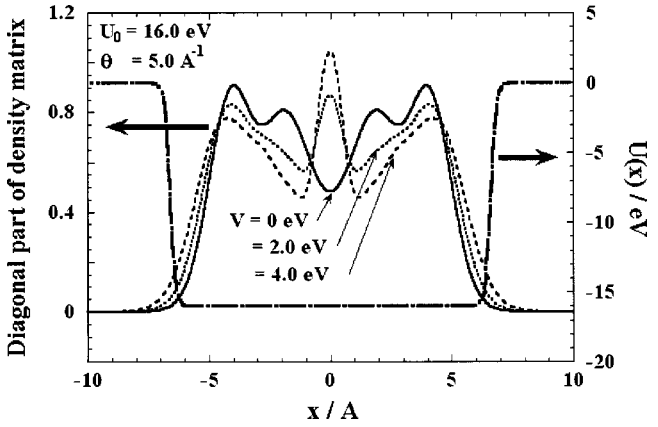


FIG. 1. One-dimensional smooth box potential $U(x)$ for the case of $U_0 = 16.0$ eV and $\theta = 5.0$ A$^{-1}$ and the diagonal part of the density matrix $\rho(x,x,t)$ of the Hartree–Fock ground state at $t=0$ fs for $V=0$, 2.0, and 4.0 eV as a function of the coordinate $x$.

Consequently, a peak grows up at the center. These features reflect the spreading of the electron cloud due to electron–electron repulsion.

In Fig. 2 we display the time evolution of the entire density matrix $\rho(x,x',t)$ in the two-dimensional plots at times 0, 40, 50, 60, and 100 fs for $V=0$ eV (left-hand side column) and $V=2.0$ eV (right-hand side). The field intensity $I=3.0\times10^{15}$ W/cm$^2$ and frequency $\Omega=1334$ cm$^{-1}$. In Fig. 2 we show small values between $-0.1$ and 0.1 by the contour maps for the entire $5L$ calculated region. The coordinate value of these figures represents the entire calculated region $5L=66.0$ A with a 100 points grid. The potential region is between 40 and 60.

We see how the externally driven charges oscillate and fluctuate in the potential region. Charge fluctuations for $V=0$ eV are larger than for $V=2.0$ eV. This is because as the Coulomb interaction is switched on, the electron motions are strongly correlated and collective. As the external field sets in, the off-diagonal elements of the density matrix in the potential region begin to fluctuate strongly. Due to the Coulombic interaction, the fluctuation for $V=2.0$ eV shows a noticeable cooperativity compared to $V=0$ eV. As the field becomes stronger, around $t=50$ fs, new off-diagonal components are induced between the potential and outer regions. Through these off-diagonal elements, the diagonal part of the outer region corresponding to the charge of the ionized electrons grows. It is also seen that the electrons are emitted from the potential to the outer region constructing the wave packets. For $V=2.0$ eV, the wave packets of the emitted electrons are bound in the potential region, as compared with the $V=0$ eV case. This comes from the Coulombic interaction between the emitted electrons and the polarization created by the fluctuation of electrons in the potential region. The oscillatory behavior in both diagonal and off-diagonal components of the density matrix lasts beyond $t=60$ fs where the external field almost vanishes. This is because dissipation processes are not included in our model, and the field-induced higher-energy nonstationary electronic state cannot dissipate its excess energy to a heat bath.

The time evolution of the off-diagonal components of the density matrix is very sensitive to the Coulomb and the exchange interaction. Hence, both play an essential role in the many-electron dynamics.

We define the ionization number as the total number of electrons that leave the potential region to the outer region,

$$(\text{Ionization number}) = \int_{-L'/2}^{+L'/2} \{\rho(x,x,0) - \rho(x,x,t)\} dx$$

$$= 8 - \int_{-L'/2}^{+L'/2} \rho(x,x,t) dx. \qquad (3.1)$$

Here, we take $L'=L+0.5$ A to be slightly larger than $L$.

We next consider the time evolution of the ionization number calculated using Eq. (3.1), as depicted in Fig. 3 as a function of time for $V=0$ eV (broken line) and $V=2.0$ eV (solid line). The field amplitude $E(t)$ for $\Omega=1334$ cm$^{-1}$ is also plotted in Fig. 3 by the dotted line. Back electron transfer from the outer to the potential region is clearly noticeable for $V=2.0$ eV around $t=50$ fs compared with $V=0$ eV. This can be attributed to Coulomb interaction between the polarization in the potential region and the ionized electrons; the ionized electrons are weakly bonded to the potential region by the interaction $V$.

### B. Dependence on field intensity

We have examined the ionization dynamics dependence on field intensity $I$ for $\Omega=1334$ cm$^{-1}$ and $V=2.0$ eV. In Fig. 4, we display the time evolution of the ionization number for various values of $I$. As $I$ exceeds about $1\times10^{15}$ W/cm$^2$, back electron transfer from the outer region becomes noticeable around $t=50$ fs. This is due to the Coulomb interaction between the ionized electrons and the remaining holes in the potential region.

In order to estimate the total number of electrons ejected from the potential region during the femtosecond laser pulse, we define the final ionization number. In Fig. 5, we display the final ionization number at $t=100$ fs as a function of $I$ by log–linear plot (solid line) and by log–log plot (dotted line). These plots show that the final ionization number scales as $\sim I^n$, and the $I$-dependence changes in the vicinity of $I=10^{15}$ W/cm$^2$. The exponent $n$ for the region below $I=10^{15}$ W/cm$^2$ is larger than above $10^{15}$ W/cm$^2$. This can be attributed to back electron transfer from the outer to the potential region occurring above $I=10^{15}$ W/cm$^2$, as seen in Fig. 4.

### C. Dependence on field frequency

We have examined the dependence of the ionization on the field frequency $\Omega$, for a fixed $I=13.2\times10^{14}$ W/cm$^2$ and $V=2.0$ eV. The time evolution of the ionization number is depicted in Fig. 6 for various values of $\Omega$. In Fig. 7, the final ionization number is plotted versus $\Omega$. We see that when $\Omega$ is lower than about 10 000 cm$^{-1}$, the final ionization number increases with $\Omega$. In this region, the ionization mechanism changes from tunneling to a nonadiabatic multielectron excitation process. At higher $\Omega$, the final ionization number rapidly decreases with $\Omega$. This can be rationalized as follows: When $\Omega \geqslant 10\,000$ cm$^{-1}$, the time period of the field oscilla-

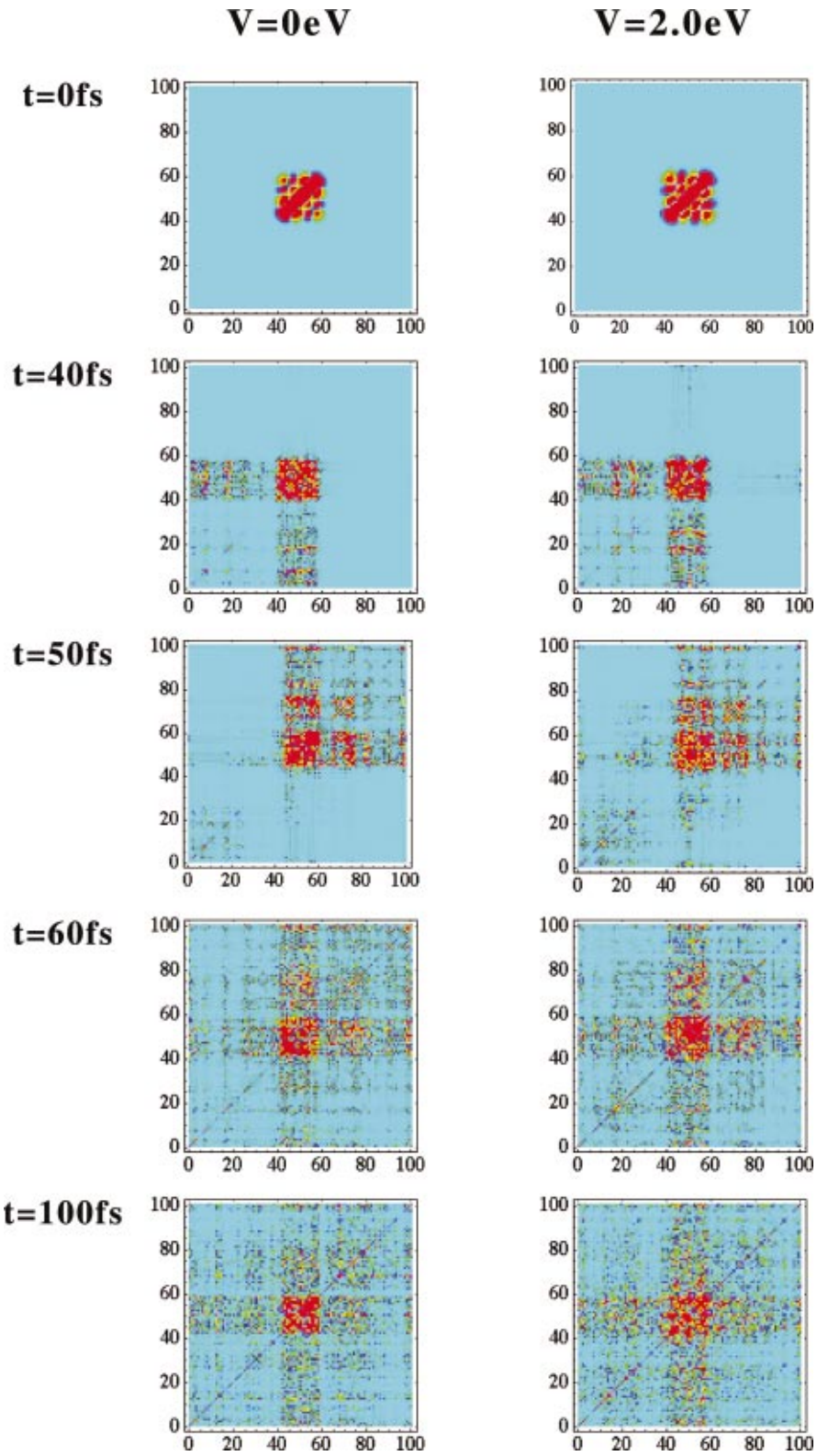


FIG. 2. (Color) Two-dimensional plots of the density matrix $\rho(x,x',t)$ of the entire calculated region at times 0, 40, 50, 60, and 100 fs. Left-hand side column is for $V=0$ eV and right-hand side for $V=2.0$ eV. $\Omega=1334$ cm$^{-1}$ and $I=3.0\times10^{15}$ W/cm$^2$.

tion exceeds the propagation time of the electron to move to the outer region. The excited electrons cannot escape from the potential region during 100 fs, and the electrons remain in the potential region for a long time.

### D. Saturation ionization intensity

We have determined the saturation ionization intensity ($I_{\mathrm{sat}}$) by extrapolating the baseline of the ionization number plotted as a function of $\log[I/(\mathrm{W/cm}^2)]$ for various values of $\Omega$, as seen in Fig. 8, and compare with the experimental results of Ivanov *et al.*[12]

$I_{\mathrm{sat}}$ versus $\lambda$ is depicted in Fig. 9. The solid circles and solid line indicate the present calculations. The crosses from the study of Ivanov *et al.*[12] are on decatetraene. The dotted line (calculated) and the open circles (observed) $I_{\mathrm{sat}}$. As discussed in the previous section, in the vicinity of $\lambda$

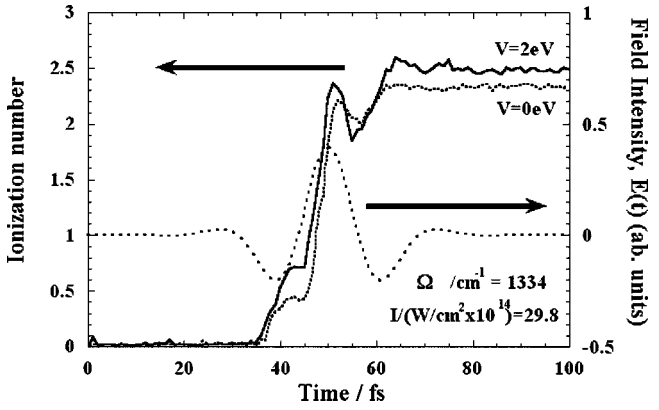


FIG. 3. Time evolution of the total number of electrons emitted from the potential region (ionization number) for $V=0$ and 2.0 eV in the case of $\Omega=1334$ cm$^{-1}$ and $I=3.0\times10^{15}$ W/cm$^2$. The dotted line is the field envelope $E(t)$ for $\Omega=1334$ cm$^{-1}$. The pulse duration $\delta=10$ fs and the center of the pulse $t_p=50$ fs.

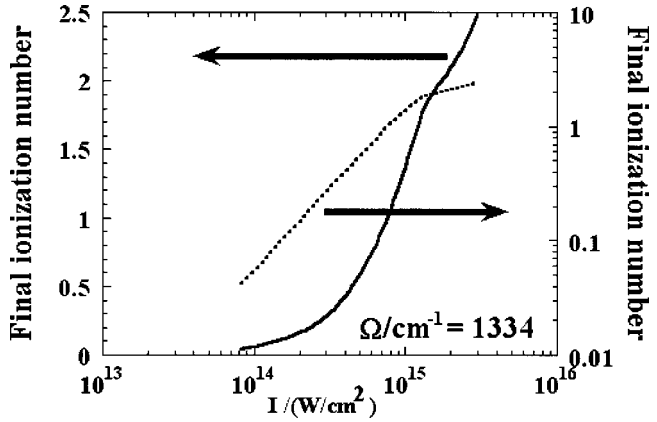


FIG. 5. Final ionization number as a function of $I$ as indicated log–linear plot (solid line) and log–log plot (dotted line). $\Omega=1334$ cm$^{-1}$ and $V=2.0$ eV.

$=1.5$ $\mu$m, the ionization dynamic is primarily determined by the tunneling process. At lower wavelengths, the ionization mechanism changes to the nonadiabatic multielectron excitation process, resulting in the decrease of $I_{\mathrm{sat}}$. Our simulations agree well with the experimental results above $\lambda=0.8$ $\mu$m. At lower wavelengths, our calculated $I_{\mathrm{sat}}$ is too high because, in this region, the time period of the field oscillation exceeds the propagation time of the excited electron and the excited electrons can not escape from the potential region during our calculation time scale of 100 fs. Our results for this region are about one order of magnitude larger than experiment. This can be rationalized as follows: Since the photon energy of the field of $\lambda=0.5$ $\mu$m is about 2.5 eV and the $\pi$-electorn energy gap of decatetraene is about 4 eV, excitons can be easily created by a few photons absorption process. To ionize the excited molecule, the multiple excitons trapped in the molecule must dissociate into electrons and holes. The time scale of this process should be longer than our calculation time scale, and is not reproduced by our simulations.

## IV. CONCLUSIONS

We have investigated many-body effects in the ionization process of polyatomic molecules with eight $\pi$-electrons, such as octatetraene or decatetraene, in a strong femtosecond laser field using a one-dimensional potential model. The time evolution of the density matrix has been calculated by numerically integrating the TDHF equations, including multielectron excitations induced by Coulomb and exchange interactions.

We have investigated the effects of the electron–electron interactions on the time evolution of the density matrix. We found that the ionized electron wave packets tend to be bound in the potential region due to the Coulombic interaction with the polarization created by the fluctuation of electrons in the potential region. We also found that the time evolution of the off-diagonal elements of the density matrix shows a noticeable cooperativity as a result of interelectron interactions, and the diagonal elements of the outer region corresponding to the charges of the ejected electrons grow through the off-diagonal elements between the potential and the outer region. These features are very sensitive to the

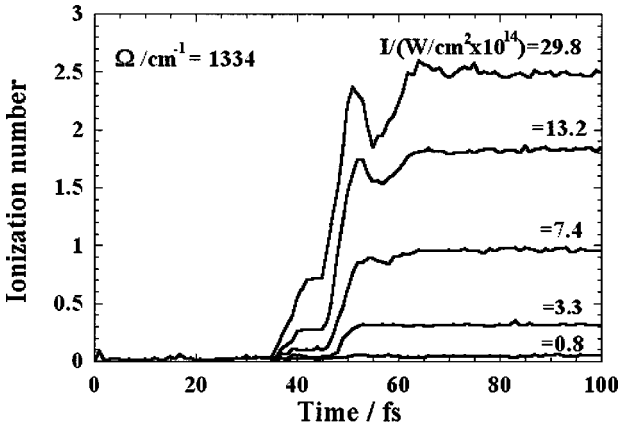


FIG. 4. Time evolution of the total number of electrons emitted from the potential region (ionization number) for various values of $I$. $\Omega=1334$ cm$^{-1}$.

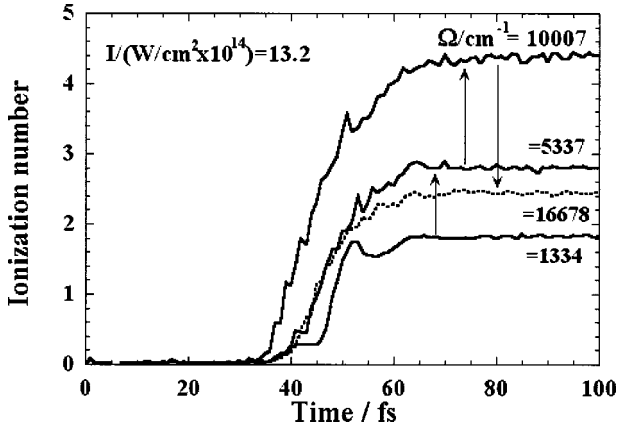


FIG. 6. The time dependent total number of electrons emitted from the potential region (ionization number) for various values of $\Omega$. $I=13.2\times10^{14}$ W/cm$^2$ and $V=2.0$ eV.

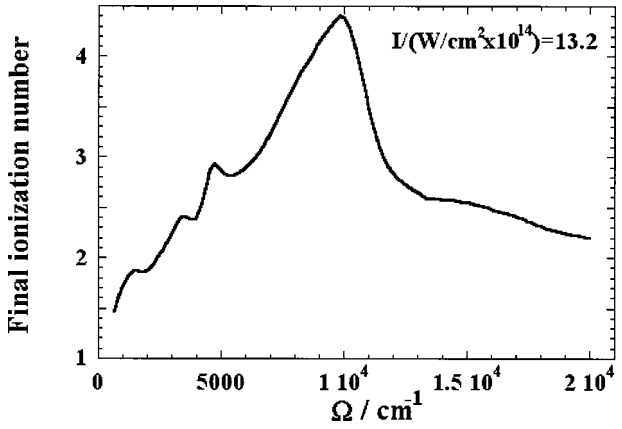


FIG. 7. Final ionization number as a function of $\Omega$ of the field for $I=13.2\times10^{14}$ W/cm$^2$ and $V=2.0$ eV.

Coulomb and exchange interactions, which control the many-electron dynamics.

We further investigated the ionization dynamics dependence on field intensity and frequency. We found that the final ionization number scales as $\sim I^n$, and the scaling exponent $n$ changes in the vicinity of $I=10^{15}$ W/cm$^2$ due to the appearance of the back electron transfer from the outer to the potential region. When $\Omega$ is less than about 10 000 cm$^{-1}$, the final ionization number increases with $\Omega$. In this region, the ionization mechanism changes from tunneling to nonadiabatic multielectron excitation. At higher frequencies, the final ionization number rapidly decreases with $\Omega$ because the excited electrons cannot escape from the potential region during our simulation time of 100 fs.

Our calculated saturation ionization intensity results agrees well with the experiment for wavelengths longer than $\lambda=0.8$ $\mu$m. For shorter wavelengths, our calculated $I_{sat}$ increases and are about one order of magnitude larger than experiment. This comes from the effect of a long-time ionization process of the excitons whose lifetime exceeds our simulation time scale.

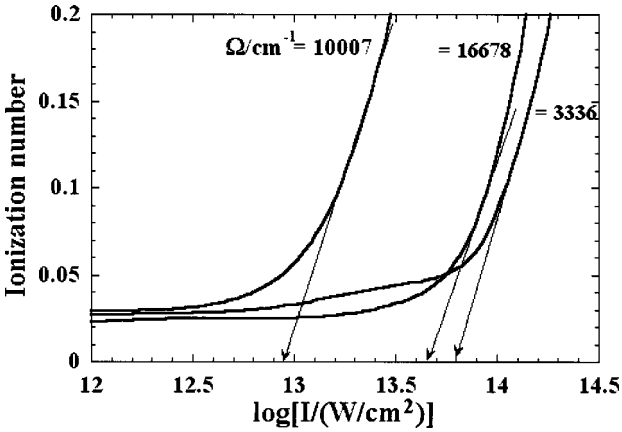


FIG. 8. Ionization number for relatively low-field intensity as a function of $\log[I/(\mathrm{W/cm^2})]$ for various values of $\Omega$. Linear extrapolation to the baseline determines the saturation intensity $I_{sat}$.

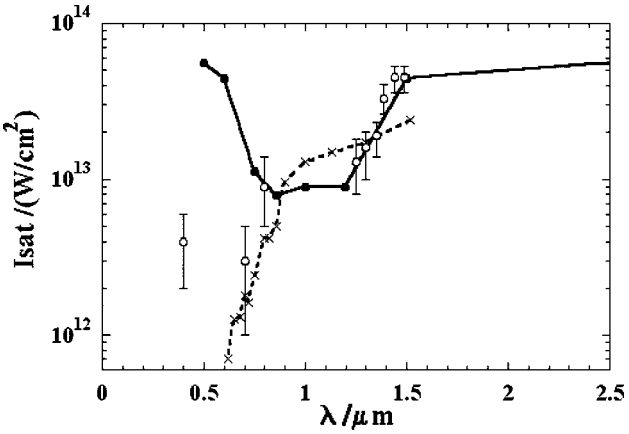


FIG. 9. Saturation intensity $I_{sat}$ as a function of field wavelength $\lambda$. The solid circles and the solid line show present calculations. The crosses and the dotted line are the calculated results and the open circles are the observed $I_{sat}$ by Ivanov *et al.* (see Ref. 12).

## ACKNOWLEDGMENTS

The support of the National Science Foundation Grant No. CHE-0132571 is gratefully acknowledged. One of the authors (M.S.) is very grateful to Professor T. Iida for his continuous support and encouragement.

[1] T. Elsaesser, S. Mukamel, M. M. Murnane, and N. F. Scherer, *Ultrafast Phenomena XII* (Springer, Berlin, 2000).
[2] "Super-Intense Laser-Atom Physics," Nato Science Series, edited by B. Piraux and K. Rzazewski (Kluwer, Dordrecht, 2001).
[3] T. Iida, M. Suzuki, and M. Aihara, J. Lumin. **66**, 483 (1996).
[4] M. J. DeWitt and R. J. Levis, Phys. Rev. Lett. **81**, 5101 (1998).
[5] M. J. DeWitt and R. J. Levis, J. Chem. Phys. **108**, 7045 (1998).
[6] M. J. DeWitt and R. J. Levis, J. Chem. Phys. **110**, 11368 (1999).
[7] S. M. Hankin, D. M. Villeneuve, P. B. Corkun, and D. M. Rayner, Phys. Rev. Lett. **84**, 5082 (2000).
[8] A. N. Markevitch, N. P. Moore, and R. J. Levis, Chem. Phys. **267**, 131 (2001).
[9] G. von Helden, I. Holleman, G. M. H. Knippels, A. F. G. van der Meer, and G. Meijer, Phys. Rev. Lett. **79**, 5234 (1997).
[10] M. Tchaplyguine, K. Hoffmann, O. Duhr, H. Hohmann, G. Korn, H. Rottke, M. Wittmann, I. V. Hertel, and E. E. B. Campbell, J. Chem. Phys. **112**, 2781 (2000).
[11] M. Lezius, V. Blanchet, D. M. Rayner, D. M. Villeneuve, A. Stolow, and M. Y. Ivanov, Phys. Rev. Lett. **86**, 51 (2001).
[12] M. Lezius, V. Blanchet, M. Y. Ivanov, and A. Stolow, J. Chem. Phys. **117**, 1575 (2002).
[13] L. V. Keldysh, Sov. Phys. JETP **20**, 1307 (1965).
[14] M. V. Ammosov, N. B. Delone, and V. P. Kraiov, Sov. Phys. JETP **64**, 1191 (1986).
[15] G. L. Yudin and M. Y. Ivanov, Phys. Rev. A **63**, 033404 (2001).
[16] G. L. Yudin and M. Y. Ivanov, Phys. Rev. A **64**, 013409 (2001).
[17] T. Seideman, M. Y. Ivanov, and P. B. Corkum, Chem. Phys. Lett. **252**, 181 (1996).
[18] A. Conjusteau, A. D. Bandrauk, and P. B. Corkum, J. Chem. Phys. **106**, 9095 (1997).
[19] I. Kawata, H. Kono, Y. Fujimura, and A. D. Bandrauk, Phys. Rev. A **62**, 031401(R) (2001).
[20] M. Thachuk, M. Y. Ivanov, and D. M. Wardlaw, J. Chem. Phys. **105**, 4094 (1996).
[21] M. Thachuk, M. Y. Ivanov, and D. M. Wardlaw, J. Chem. Phys. **109**, 5747 (1998).
[22] M. Suzuki and S. Mukamel, J. Chem. Phys. **119**, 4722 (2003).
[23] K. C. Kulander, Phys. Rev. A **36**, 2726 (1987).
[24] K. C. Kulander, Phys. Rev. A **38**, 778 (1988).
[25] M. S. Pindzola, D. C. Griffin, and C. Bottcher, Phys. Rev. Lett. **66**, 2305 (1991).

[26] M. S. Pindzola, P. Gavras, and T. W. Gorczyca, Phys. Rev. A **51**, 3999 (1995).
[27] M. S. Pindzola, F. Robicheaux, and P. Gavras, Phys. Rev. A **55**, 1307 (1997).
[28] S. Tretiak and S. Mukamel, Chem. Rev. (Washington, D.C.) **102**, 3171 (2002).
[29] J. C. Butcher, *The Numerical Analysis of Ordinary Differential Equations* (Wiley, New York, 1987).